Alkane Oxidation Catalyzed by μ-Oxo-Bridged Diferric Complexes: A Structure/Reactivity Correlation Study

Stéphane Ménage,† Jean Marc Vincent,† Claude Lambeaux,† Geneviève Chottard,‡ André Grand,§ and Marc Fontecave*,†

Laboratoire d'Etudes Dynamiques de la Structure et de la Sélectivité, URA 332, Université Joseph Fourier, BP 53X, 38041 Grenoble Cedex, France, Laboratoire de Chimie des Métaux de Transition, URA 419, Université Paris VI, 75252 Paris Cedex 05, France, and Laboratoire DRFMC/SESAM/CC, Centre d'Etudes Nucléaires de Grenoble, F-85X 38041 Grenoble Cedex, France

Received January 14, 1993®

A series of μ-oxo-bridged diferric complexes, $Fe_2OL_4X_n(ClO_4)_m$, containing two bidentate nitrogen ligands (L = 2,2′-bipyridine, 4,4′-dimethyl-2,2′-bipyridine, and 1,10-phenanthroline) and one exchangeable coordination site (X = H_2O, Cl, CH_3CO_2, CF_3CO_2) per iron were synthesized and characterized by their ^1H NMR, electronic, and Raman spectra and by their magnetic properties. ^1H NMR data showed that X = H_2O or X = bridging CH_3CO_2 were labile ligands while X = Cl was much less exchangeable. Complex **3D** (L = 4,4′-dimethyl-2,2′-bipyridine, X = CF_3CO_2, n = 2, m = 2) was characterized crystallographically. The complexes were found to catalyze the oxidation of cyclohexane, adamantane, toluene, benzyl alcohol, and *trans*-stilbene by *tert*-butyl hydroperoxide. Functionalization of cyclohexane gave cyclohexanol and cyclohexanone in nearly equal relative amounts together with small amounts of *tert*-butylcyclohexyl peroxide. The C3/C2 ratio, determined during adamantane oxidation, was around 10. Product yields, turnover numbers, and stability of the catalyst could be finely tuned by small modifications, both at the nitrogen ligand and at the exchangeable coordination site. In particular, the more labile the X ligand, the more effective the catalyst. Complex **2A** (L = 2,2′,-bipyridine, X = H_2O, n = 2, m = 4) was the most effective catalyst with a turnover number of 16 per minute during cyclohexane oxidation. This is among the highest values reported so far during oxidation of hydrocarbons by TBHP catalyzed by a non-heme iron complex.

Introduction

Binuclear oxo-bridged non-heme iron complexes (containing the Fe–O–Fe unit) have recently received much attention.[1] They provide structural models for diiron sites in proteins involved in the storage (hemerythrin, Hr) or the reductive activation (ribonucleotide reductase, RNR; methane monooxygenase, MMO) of molecular oxygen. Crystallographic studies have unambiguously demonstrated the presence of such a binuclear iron center only in the case of Hr[2] and RNR.[3] Coordination sites were shown to be available for binding exogenous ligands, in particular molecular oxygen.[4] In the case of MMO, for which a refined three-dimensional structure is not available, recent spectroscopic studies have raised the possibility that, instead, the iron ions are hydroxo-bridged.[5] On the other hand, sequence homologies between RNR and MMO have led to a model of the diiron site in MMO very similar to that of RNR.[6] While the iron center of RNR is involved in the one-electron oxidation of a tyrosine residue of the active site, that of MMO is active in the oxidation of a variety of alkanes, including methane.[7] Very recently, it has been shown that both systems can use single oxygen atom donors such as hydrogen peroxide instead of oxygen and electrons for enzymatic activity.[8]

Alkane functionalization is still a major challenge for organic chemistry. There is still a need for new efficient and selective catalysts for alkane oxidation. However, the ability of model complexes of MMO or RNR, containing the Fe–O–Fe motif, to catalyze the oxidation of hydrocarbons has received very little attention. Such studies include the following systems:[9] $Fe_2O(OAc)_2(bipy)_2Cl_2$/TBHP[10] and $Fe_2O(OAc)_2(bipy)_2Cl_2$ or $[Fe_2O(OAc)(tmima)_2](ClO_4)_3/H_2O_2$,[11] $Fe_2O(HB(pz)_3)_2(hfcac)_2$/Zn/$O_2$ and $Fe_2O(HB(pz)_3)_2(OAc)_2$/Zn/O_2,[12] $Fe_2(TPA)_2O(ClO_4)_4/H_2O_2$,[13] $Fe_2(salen)_2O$/2-mercaptoethanol/O_2,[14] and $Fe_2O(Phen)_4(OH_2)_2(ClO_4)_4$/TBHP.[15]

† Université Joseph Fourier.
‡ Université Paris VI.
§ Centre d'Etudes Nucléaires de Grenoble.
® Abstract published in *Advance ACS Abstracts*, September 1, 1993.

(1) (a) Que, L., Jr.; True, A. E. *Prog. Inorg. Chem.* **1990**, *38*, 97. (b) Sanders-Loehr, J. In *Iron Carriers and Iron Proteins*; Loehr, T. M.; Ed.; VCH Publishers: New York, 1989; p 373. (c) Que, L., Jr.; Scarrow, R. C. *ACS Symp. Ser.* **1988**, *372*, 152. (d) Kurtz, D. M., Jr. *Chem. Rev.* **1990**, *90*, 585.
(2) (a) Stenkamp, R. E.; Sieker, L. C.; Jensen, L. H. *J. Am. Chem. Soc.* **1984**, *106*, 618. (b) Sheriff, S.; Hendrickson, W. A.; Smith, J. L. *J. Mol. Biol.* **1987**, *197*, 273.
(3) Nordlund, P.; Sjöberg, B.-M.; Eklund, H. *Nature* **1990**, *345*, 593.
(4) Stenkamp, R. E.; Sieker, L. C.; Jensen, L. H.; McCallum, J. D.; Sanders-Loehr, J. *Proc. Natl. Acad. Sci. U.S.A.* **1985**, *82*, 713.
(5) DeWitt, J. G.; Bentsen, J. G.; Rosenzweig, A. C.; Hedman, B.; Green, J.; Pilkington, S.; Papaefthymiou, G. C.; Dalton, H.; Hodgson, K. O.; Lippard, S. J. *J. Am. Chem. Soc.* **1991**, *113*, 9219.
(6) Nordlund, P.; Dalton, H.; Eklund, H. *FEBS letters* **1992**, *307*, 257.
(7) (a) Green, J.; Dalton, H. *Biochem. J.* **1986**, *236*, 155. (b) Shimoda, M.; Ono, M.; Okura, I. *J. Mol. Catal.* **1989**, *52*, L37.
(8) MMO: Anderson, K. K.; Froland, W. A.; Lee, S.-K.; Lipscomb, J. D. *New J. Chem.* **1991**, *15*, 411. RNR: Fontecave, M.; Gerez, C.; Atta, M.; Jeunet, A. *Biochem. Biophys. Res. Commun.* **1990**, *168*, 659.
(9) Abbreviations used: TBHP, *tert*-butyl hydroperoxide; TPA; tris(2-pyridylmethyl)amine; tmima, tris(1-methylimidazol-2-yl)amine; BIPhMe, bis(1-methylimidazol-2-yl)phenylmethoxymethane; bipy, 2,2′-bipyridine; salen, N,N′-ethylenebis(salicyclideneaminato); hfacac, hexafluoroacetylacetone; OAc, acetate; phen, *o*-phenanthroline; 44′Me$_2$-22′bipy, 4,4′-dimethyl-2,2′-bipyridine; HB(pz)$_3$, hydrotris(pyrazolyl)-borate; CyOOtBu = *tert*-butyl cyclohexyl peroxide, CyOH, cyclohexanol; CyONE, cyclohexanone; MeOH, methanol.
(10) Vincent, J. B.; Huffman, J. C.; Christou, G.; Li., Q.; Nanny, M. A.; Hendrickson, D. N.; Fong, R. H.; Fish, R. H. *J. Am. Chem. Soc.* **1988**, *110*, 6898.
(11) Fish, R. H.; Konings, M. S.; Oberhausen, K. J.; Fong, R. H.; Yu, W. M.; Christou, G.; Vincent, J. B.; Coggin, D. K.; Buchanan, R. M. *Inorg. Chem.* **1991**, *30*, 3002 and references therein.
(12) (a) Kitajima, N.; Fukui, H.; Moro-oka, Y. *J. Chem. Soc., Chem. Commun.* **1988**, 485. (b) Kitajima, N.; Ito, M.; Fukui, H.; Moro-oka, Y. *J. Chem. Soc., Chem. Commun.* **1991**, 102.
(13) Leising, R. A.; Brennan, B. A.; Que, L., Jr.; Fox, B. G.; Münck, E. *J. Am. Chem. Soc.* **1991**, *113*, 3988.

0020-1669/93/1332-4766$04.00/0

In this paper, we report the preparation and characterization of new Fe–O–Fe model complexes, and their catalytic properties during oxidation of hydrocarbons by *tert*-butyl hydroperoxide, a monooxygen transfer reagent. The complexes have been designed for presenting one exchangeable coordination site per iron, in order to allow oxidants or substrates to interact with the ferric ion of the catalyst. The coordination sphere of each iron is completed by two bidentate nitrogen ligands. This is the first study that is aimed to correlate the catalytic activity of binuclear μ-oxo-bridged iron complexes to their structure.

Experimental Procedures

Synthetic Methods. *tert*-Butyl cyclohexyl peroxide was synthesized according to literature procedure[16] while all other chemicals were purchased commercially and used as received. *Caution! The perchlorate salts in this study are all potentially explosive and should be handled with care.* The $Fe_2OL_4X_n(ClO_4)m$ complexes were prepared as follows.

Synthesis of $Fe_2O(L)_4(H_2O)_2(ClO_4)_4$. $Fe_2O(C_{12}H_8N_2)_4(H_2O)_2(ClO_4)_4\cdot 3H_2O$ (**1A**) was synthesized according to literature procedure using $Fe(ClO_4)_3\cdot 9H_2O$ as the iron salt.[17] For complex **3A**, the same procedure was effective using methanol instead of water as the solvent.

A modified procedure was required for the preparation of complex **2A**: 2 mmol of bipyridine was added to 1 mmol of $Fe(ClO_4)_3\cdot 9H_2O$ in 20 mL of methanol. The original solution turned deep green after adding 1 mmol of Et_3N (140 μL). Immediately a turbid solution resulted which became darker and nonturbid with time. The solution was then left at −18 °C and afforded a green powder with satisfactory analysis. The water ligand comes from the ferric salt.

Anal. Calcd for $Fe_2O(C_{10}H_8N_2)_4(H_2O)_2(ClO_4)_4\cdot 2H_2O$ ($C_{40}H_{40}Cl_4Fe_2N_8O_{21}$) (**2A**): C, 39.31; H, 3.27; N, 9.17; Cl, 11.60; Fe, 9.14. Found: C, 39.26; H, 3.16; N, 9.02; Cl, 11.59; Fe, 9.18.

Anal. Calcd for $Fe_2O(C_{12}H_{12}N_2)_4(H_2O)_2(ClO_4)_4\cdot 3H_2O$ ($C_{48}H_{58}Cl_4Fe_2N_8O_{22}$) (**3A**): C, 42.64; H, 4.29; N, 8.28; Cl, 10.49; Fe, 8.26. Found: C, 42.69; H, 4.27; N, 8.18; Cl, 10.42; Fe, 8.26.

Caution! Sometimes an impurity, identified as $Fe^{II}(L)_3(ClO_4)_2$, precipitated with the expected products during the recrystallization by slow diethyl ether diffusion in an acetonitrile solution.

Synthesis of $Fe_2OL_4(CH_3CO_2)(ClO_4)_3$. A 1-mmol sample of $Fe(ClO_4)_3\cdot 9H_2O$ (520 mg) and 1 mmol of sodium acetate were mixed together in methanol (10 mL). A solution of the ligand L (2 mmol) in acetonitrile (5–10 mL) was added to the resulting brown solution. The solution turned green brown, and a precipitated appeared after 5 min. For **2B**, a microcrystalline powder appeared when the mother liquor was left at −18 °C. Recrystallization by slow ethyl acetate diffusion in acetonitrile solution was effective for **1B** and **3B**. This procedure afforded satisfactory analysis.

Anal. Calcd for $Fe_2O(C_{12}H_8N_2)_4(CH_3CO_2)(ClO_4)_3\cdot H_2O$ ($C_{50}H_{37}Cl_3Fe_2N_8O_{16}$) (**1B**): C, 49.08; H, 3.02; N, 9.15; Cl, 8.69; Fe, 9.12. Found: C, 49.01; H, 3.16; N, 8.73; Cl, 8.86; Fe, 9.01.

Anal. Calcd for $Fe_2O(C_{10}H_8N_2)_4(CH_3CO_2)(ClO_4)_3\cdot 2H_2O$ ($C_{42}H_{39}Cl_3Fe_2N_8O_{17}$) (**2B**): C, 44.03; H, 3.40; N, 9.78; Cl, 9.28; Fe, 9.75. Found: C, 43.96; H, 3.53; N, 9.49; Cl, 8.90; Fe, 10.34.

Anal. Calcd for $Fe_2O(C_{12}H_{12}N_2)_4(CH_3CO_2)(ClO_4)_3\cdot 3H_2O\cdot C_4H_8O_2$ ($C_{54}H_{65}Cl_3Fe_2N_8O_{20}$) (**3B**): C, 47.56; H, 4.76; N, 8.21; Cl, 7.79; Fe, 8.19. Found: C, 47.27; H, 4.71; N, 8.21; Cl, 8.50; Fe, 8.56.

Synthesis of $Fe_2O(L)_4(Cl)_2(ClO_4)_2$. To a methanolic solution (10 mL) of 1 mmol of $FeCl_3\cdot 6H_2O$ the ligand L was added as a solid. The orange solution turned deep brown. A brown precipitate immediately appeared after addition of an excess of sodium perchlorate. Recrystallization by slow ethyl acetate diffusion in acetonitrile solution afforded a complex with satisfactory analysis.

Anal. Calcd for $Fe_2O(C_{12}H_8N_2)_4(Cl)_2(ClO_4)_2\cdot 3H_2O$($C_{48}H_{38}Cl_4Fe_2N_8O_{12}$) (**1C**): C, 49.10; H, 3.23; N, 9.60; Cl, 12.10; Fe, 9.53. Found: C, 48.74; H, 3.12; N, 9.57; Cl, 12.00; Fe, 9.46.

Anal. Calcd for $Fe_2O(C_{10}H_8N_2)_4(Cl)_2(ClO_4)_2\cdot 4H_2O$ ($C_{40}H_{40}Cl_4Fe_2N_8O_{13}$) (**2C**): C, 43.90; H, 2.93; N, 10.26; Cl, 13.00; Fe, 10.22. Found: C, 43.83; H, 2.89; N, 10.19; Cl, 13.63; Fe, 10.08.

Anal. Calcd for $Fe_2O(C_{12}H_{12}N_2)_4(Cl)_2(ClO_4)_2$ ($C_{48}H_{48}Cl_4Fe_2N_8O_9$) (**3C**) C, 50.91; H, 4.23; N, 9.90; Cl, 12.52; Fe, 9.8. Found: C, 50.73; H, 3.96; N, 9.94; Cl, 12.52; Fe, 9.25.

Synthesis of $Fe_2O(L)_4(CF_3CO_2)_2(ClO_4)_2$. A 1-mmol sample of $Fe(ClO_4)_3\cdot 9H_2O$ (520 mg) and a mixture of 2 mmol of trifluoroacetic acid and 2 mmol of Et_3N were mixed together in methanol (10 mL). The ligand L (2 mmol) was then added as a solid to the resulting brown solution. Immediately, a green precipitate was obtained.

Anal. Calcd for $Fe_2O(C_{12}H_8N_2)_4(CF_3CO_2)_2(ClO_4)_2\cdot H_2O$ ($C_{52}H_{34}F_6Cl_2Fe_2N_8O_{14}$) (**1D**): C, 48.41; H, 2.63; N, 8.68; Cl, 5.5; Fe, 8.65; F, 8.83. Found: C, 48.55; H, 2.83; N, 8.50; Cl, 6.02; Fe, 8.4; F, 8.20.

Anal. Calcd for $Fe_2O(C_{10}H_8N_2)_4(CF_3CO_2)_2(ClO_4)_2\cdot H_2O$ ($C_{44}H_{34}F_6Cl_2Fe_2N_8O_{14}$) (**2D**): C, 44.2; H, 2.89; N, 9.37; Cl, 5.93; Fe, 9.34; F, 9.53. Found: C, 43.72; H, 2.54; N, 9.30; Cl, 5.97; Fe, 9.34; F, 9.08.

Anal. Calcd for $Fe_2O(C_{12}H_{12}N_2)_4(CF_3CO_2)_2(ClO_4)_2\cdot 3H_2O$ ($C_{52}H_{54}F_6Cl_2Fe_2N_8O_{16}$) (**3D**): C, 46.5; H, 4.02; N, 8.34; Cl, 5.97; Fe, 8.40; F, 8.40. Found: C, 46.3; H, 3.9; N, 8.18; Cl, 6.5; Fe, 7.80; F, 7.64.

Crystallographic Results for $[Fe_2O(C_{12}H_{12}N_2)_4(CF_3CO_2)_2](ClO_4)_2\cdot C_4H_8O_2$ (3D). X-ray diffraction data were collected on a dark green parallelepipedic crystal of $[Fe_2O(C_{12}H_{12}N_2)_4(CF_3CO_2)_2](ClO_4)_2\cdot C_4H_8O_2$ of approximate dimensions 0.2 × 0.2 × 0.2 mm using an Enraf-Nonius CAD4 diffractometer with monochromatized Mo Kα radiation. Crystal data, together with details of the diffraction experiment and subsequent calculations, are listed in Table III. The cell dimensions were obtained by least-squares refinement of the setting angles for 25 reflections ($2\theta > 10°$). The stability of the crystal was monitored during data collection by measuring the intensities of three control reflections after every 3600 s of exposure time. No significant trend in these intensities was observed during the course of data acquisition. Lorentz and polarization but no absorption corrections were applied to the data.

The structure was solved by conventional Patterson and Fourier methods using Shelx-86 package,[18] which led to the location of all the non-H atoms. Structure refinements were carried out by full-matrix least-squares methods with anisotropic thermal parameters using scattering factors from ref 19 and included anomalous dispersion terms.[20] Hydrogen atoms were included in calculated positions (C–H = 1.08 Å). Weighted ($w = [\sigma^2(F)]^{-1}$) least-squares refinements on F were carried out by alternately refining half by half of the molecule, followed by the anions and finally the solvent molecule, and led to final values of $R = 0.083$ and $R_w = 0.063$ [$R = (\sum|F_o - F_c|)/(\sum F_o)$; $R_w = \{(\sum w|F_o - F_c|^2)/(\sum w(F_o)^2)\}^{1/2}$. A Final Fourier difference map showed no significant electron density.

Fluoromethyl groups were affected by a large temperature factor which reflected their ability to rotate. The solvent molecule presented a dynamical disorder which did not allow a good positioning of all the atoms but did not affect the precision of the position parameters for the cationic part of the molecule. The structure of the cation $[Fe_2O(C_{12}H_{12}N_2)_4(CF_3CO_2)_2]^{2+}$ is shown in Figure 4, together with the numbering scheme for the complex. The final fractional coordinates for **3D** are contained in Table S2 (supplementary material), while selected bond lengths and angles are reported in Table IV. A complete listing of bond lengths and angles and thermal parameters is included in the supplementary material.

Physical Methods. Visible spectra were recorded on a Uvikon 930 spectrophotometer. ^1H and ^{19}F NMR spectra were recorded on a Bruker WP 200 spectrophotometer at 200 MHz. Chemical shifts (ppm) were referred to residual protic solvent peaks. The resonance Raman spectra were obtained on a J.Y. U_{1000} double monochromator, equipped with an RCA C31034 photomultiplier and photon-counting detection. The 413.1-nm exciting line of a Kr^+ laser was used at a 10-mW power level. The spectral slit width was fixed at 6 cm^{-1}. The solutions (4–6 mM in CH_3CN) were examined in a rotating cuvette to prevent photodegradation. Subtraction of the solvent bands was carried but using a spectrum of the pure solvent, recorded under the same conditions and normalized on the 920-cm^{-1} band. EPR spectra were recorded with a Varian E102 at T = 4 K. Elemental analyses were obtained from Laboratoire de Microanalyse Lyon, France. Magnetic susceptibility data were recorded over a temperature range of 5–300 K at a measuring field of 2000 G for **1C** and 5000 G for **2B** with a Quantum Design superconducting SQUID susceptometer. Gas chromatography was performed on a Perkin-Elmer

(14) Tabushi, I.; Nakajima, T.; Seto, K. *Tetrahedron Lett.* **1980**, *21*, 2565.
(15) Fontecave, M.; Roy, B.; Lambeaux, C. *J. Chem. Soc., Chem. Commun.* **1991**, 939.
(16) Bloodworth, A. J.; Courtneidge, J. L. *J. Chem. Soc. Perkin Trans. 1* **1982**, 1797.
(17) Plowman, J. E.; Loehr, T. M.; Schauer, C. K.; Anderson, O. P. *Inorg. Chem.* **1984**, *23*, 3553.
(18) Sheldrick, G. M. SHELX-86 system of computing programs. University of Cambridge, England, 1986.
(19) Cromer, D. T., Waber, J. T. *International Tables for X-ray Crystallography*; Kynoch Press: Birmingham, England, 1974; Vol. IV, Table 2.2 A.
(20) Cromer, D. T. *International Tables for X-ray Crystallography*; Kynoch Press: Birmingham, England, 1974; Vol. IV, Table 2.3.1.

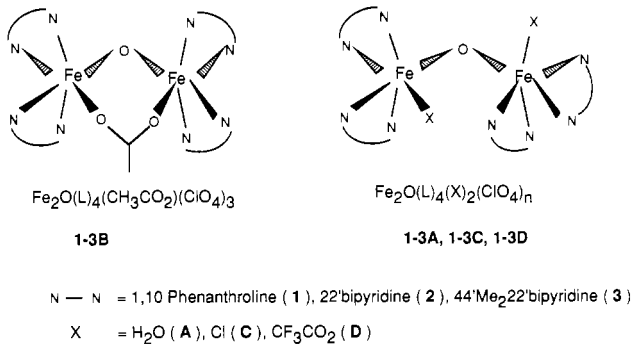

Figure 1. Schematic representation of complexes **1–3**.

Autosystem instrument connected to a Shimadzu Chromatopac CR6A with an FID detector using an OV 17 column for adamantane oxidation products and a BP 20 capillary column in the case of the other substrates.

Cyclohexane Oxidations. Standard reactions were carried out under inert atmosphere (Ar) as follows. Complexes **1A-D**, **2A-D**, and **3A-D** (3.5 μmol) were dissolved in 4.5 mL of CH_3CN containing 3.83 mmol of cyclohexane. The reaction was started by adding 0.5 mmol of TBHP (ratio of Fe_2 complex/cyclohexane/TBHP = 1/1100/140). In some experiments, argon was continuously bubbled through the solution during the reaction or reduced pressure (30–40 mmHg) was continuously applied to the reaction mixture. After 30 min or 2 h of stirring, 50 μmol of an internal standard (acetophenone) were added to the reaction mixture, and the organic products, as well as TBHP, were quantified by GC and verified by GC/MS. Unambiguous identification of the products was made by comparison with pure compounds, prepared independently or commercially available. The reaction mixture, with complex **1A** as catalyst, was assayed after an 8-min reaction for the presence of cyclohexyl hydroperoxide by ^{13}C NMR spectroscopy according to ref 11. The kinetics of the reaction were also studied by GC analysis of aliquots (0.1 mL) of the reaction mixture after treatment with 0.3 mL of diethyl ether, every first minute. The internal standard was added to the starting solution and shown to be chemically inert during the reaction.

Adamantane Oxidations. A 400-μmol sample of adamantane was oxidized by 0.5 mmol of TBHP in 4 mL of CH_3CN and 1 mL of benzene (used to obtain a homogeneous medium) containing 3.5 μmol of complex (ratio Fe_2 complex/adamantane/TBHP/1:115:140). The same protocols were applied for anaerobiosis. Oxidation products were analyzed as for cyclohexane, after a 30-min reaction.

***trans*-Stilbene Oxidation.** A 1.05-mmol sample of the alkene was added to 4.7 mL of CH_3CN and 0.25 mmol of TBHP (ratio Fe_2 complex/alkene/TBHP = 1:300:70). The reaction was completed after 15 min.

Primary Isotope Effect. Under an inert atmosphere, 1.7 μmol of complex dissolved in CH_3CN (2.4 mL) was stirred with 0.92 mmol (100 μL) each of cyclohexane and cyclohexane-d_{12}. TBHP (0.25 mmol) was then added and the solution stirred for 30 min (ratio of Fe_2 complex/cyclohexane/cyclohexane-d_{12}/TBHP = 1/550/550/140). The product yields were measured by GC (acetophenone as standard). k_H/k_D for cyclohexanol and cyclohexanone formation was obtained from the cyclohexanol/cyclohexanol-d_{12} and the cyclohexanone/cyclohexanone-d_{12} ratios, respectively.

Results

Spectroscopic Characterization of the $Fe_2OL_4X_n(ClO_4)_m$ Binuclear Iron Complexes. New μ-oxo-bridged diferric complexes with bidentate nitrogen ligands L (L = 1,10-phenanthroline, 2,2′-bipyridine, 4,4′-dimethyl-2,2′-bipyridine) have been prepared. ^1H NMR, UV–visible, and Raman resonance spectroscopies as well as magnetic studies are in full agreement with the presence of the Fe-O-Fe motif, in solution. The complexes, shown in Figure 1, have the general composition $Fe_2OL_4X_2(ClO_4)_m$ (X = OH_2, m = 4; X = Cl, m = 2; X = CF_3CO_2, m = 2) or $Fe_2OL_4X(ClO_4)_3$ (X = CH_3CO_2). All the complexes have been prepared by allowing 2 equiv of L to react with the appropriate ferric salt in MeOH, sometimes in the presence of a carboxylate salt (autoassembling method). In no case, has evidence for MeOH being bound to iron been found (the ^1H NMR spectra of the complexes either prepared in MeOH or in H_2O were found to be identical).

The cation of complexes **1A** and **1C** has been previously characterized by X-ray crystallography.[17,21] They both possess an Fe–O–Fe motif, with an Fe–O bond length of 1.787 Å. The Fe–O–Fe angle is 155.1(4) and 161(1)° for **1A** and **1C**, respectively. The iron coordination sphere is completed by four nitrogen atoms from two, 1,10-phenanthroline ligands and one water molecule for **1A** and one chloride ion for **1C**. We have determined the three-dimensional structure of complex **3D** by X-ray crystallography and found the same structure with one monodentate trifluoroacetate bound to each iron. We propose a similar structure for all complexes **A**, **C**, and **D**. In the case of complexes **B**, only one acetate is bound to the diferric unit. Their spectroscopic properties unambiguously demonstrate a bidentate bridging coordination mode for the carboxylate.

^1H NMR Studies. ^1H NMR spectroscopy has been shown to be a powerful method for probing the structural and magnetic properties of μ-oxo-bridged diferric complexes.[22] With pyridine ligands, the spectrum of such complexes was shown to display an isotropic shift pattern with broad features in the 0–40 ppm range attributed to the pyridine ring protons.[23] This range is consistent with the large antiferromagnetic coupling between the two paramagnetic centers ($|J| > 100$ cm^{-1}, $\mathcal{H} = -2JS_1 \cdot S_2$).

Complexes **1–3** exhibited closely related ^1H NMR characteristics with the isotropically shifted signals spanning a range of about 40 ppm, in agreement with the expected μ-oxo diferric structure (Table I and Figure 2). The assignments were made on the basis of T_1 measurements and ligand substitutions and by comparison to the assignments previously proposed for the μ-oxo–μ-acetato-dibridged complex **4**, $Fe_2O(TPA)_2(CH_3CO_2)(ClO_4)_3$.[24] Spectra of complexes **1A-C** (L = 1,10-phenanthroline) are shown in Figure 2. Four groups of protons were observed. Between 20 and 40 ppm, a very broad signal had the shortest T_1 values (T_1 < 1.5 ms) and was attributed to the α protons of the pyridine ring, which are the closest ones to the magnetic metal center. Signals between 12 and 20 ppm and those between 6 and 9 ppm were attributed to the β protons (T_1 around 4 ms) and to the γ protons (T_1 around 10 ms), respectively. In the spectra of complexes **3**, the latter region was featureless since the γ protons are substituted by methyl groups. The δ protons of the phenyl ring of the phenanthroline ligands were shifted between 10 and 12 ppm with large T_1 values (>15 ms). This last assignment was confirmed by the absence of resonances in this region in the case of complexes **2** and **3** and by the observation of additional features in the same region when 4,4′-diphenyl-1,10-phenanthroline was used as a ligand (data not shown).

In the spectra of complexes **B**, an extra resonance was observed, which disappeared when CH_3CO_2 was replaced by CD_3CO_2. It has thus been assigned to the protons of the iron-bound acetate group (Table I). The chemical shift value was similar to that of the bidentate bridging acetate in complex **4** but larger than that found in other complexes (δ_{OAc} ranging from 9.8 to 10.9 ppm).[24]

Finally, binding of CF_3CO_2 to iron in complex **1D** has been demonstrated by ^{19}F NMR spectroscopy. The spectrum displayed only one peak at −59.5 ppm downfield shifted with respect to trifluoroacetic acid as a standard (−72 ppm) and broadened, in agreement with the proximity of the trifluoroacetate group to the paramagnetic center.

Interestingly, for any given L ligand (for example in Figure 2, L = 1,10-phenanthroline), the complexity of the ^1H NMR spectrum was dependent on the X ligand. In complex **1B**, the eight α protons were magnetically equivalent and appeared as a

(21) Healy, P. C.; Skelton, B. W.; White, A. H. *Austr. J. Chem.* **1983**, *36*, 2057.
(22) See for example the following reference and references therein: Wu, F.-J.; Kurtz, D. M. *J. Am. Chem. Soc.* **1989**, *111*, 6563.
(23) Norman, R. E.; Yan, S.; Que, L., Jr.; Backes, G.; Ling, J.; Sanders-Loehr, J.; Zhang, J. H.; O'Connor, C. J. *J. Am. Chem. Soc.* **1990**, *112*, 1554.
(24) Yan, S.; Cox, D. D.; Pearce, L. L.; Juarez-Garcia, C.; Que, L., Jr.; Zhang, J. H.; O'Connor, C. J. *Inorg. Chem.* **1989**, *28*, 2507.

Table I. ^{1}H NMR Parameters (ppm) of $Fe_2O(L)_4(X)_n(ClO_4)$ *m* (δ(int) [T_1]) in Acetonitrile

complex	α-pyH	β-pyH	γ-pyH	δ-pyH or δ-CH_3[b]	CH_3CO_2
1A	37.0 (1), 30.8 (4)	18.1 (sh) [3.7], 16.9 (6) [4.4], 12.9 (2) [3.3]	8.4 (6) [10.3], 6.9 (2) [10.9]	11.6 (6) [13.2], 10.4 (2) [19.7]	
1B	25.3 (5)	15.3 (8) [5.1]	7.9 (8) [11.4]	11.2 (8) [15.9]	13.3 (<3) [3]
1C	28.2 (3)	17.1 (2) [5.2], 16.6 (2) [5.2], 14.9 (2) [4.6], 12.1 (2) [5.7]	8.6 (2) [11.0], 8.1 (2) [12.3], 7.8 (2) [10.8], 7.3 (2) [10.0]	11.2 (2) [15.8], 10.8 (4) [15.2], 9.8 (2) [15.5]	
1D	28.2 (2)	17.3 (2) [4.4], 16.4 (2) [5.1], 15.8 (2) [4.3], 12.6 (2) [4.0]	8.6 (2) [10.7], 8.2 (4) [11.1], 6.8 (2) [9.4]	11.3 (6) [14.2], 10.2 (2) [15.5]	
2A	30.4 (2)	19.3 (6), 16.8 (6), 15.0 (2), 12.9 (2)	7.6, 7.0[a]		
2B	24.4 (3)	17.8 (8), 15.0 (8)	7.2 (8)		13.6 (<3)
2C	27.1 (3)	18.6 (4), 17.7 (2), 16.6 (4), 15.0 (2), 14.2 (2), 12.3 (2)	8.2 (2), 7.8 (2), 7.5 (2), 6.8 (2)		
2D	27.1 (2)	18.7 (6), 16.6 (2), 16.0 (2), 15.6 (2), 14.4 (2), 12.5 (2)	8.0 (2), 7.6 (4), 6.3 (2)		
3A	28.5 (4)	18.5 (6), 16.0 (6), 15.4 (2), 12.9 (2)		5.4, 3.1	
3B	24.5 (6)	17.5 (8), 14.8 (8)		3.8	13.8 (3)
3C	26.2 (3)	17.9 (4), 17.1 (2), 16.0 (4), 14.5 (2), 13.7 (2), 11.9 (2)		4.6, 3.2	
3D	27.7 (2)	18.1 (6), 15.4 (6), 13.9 (2), 12.1 (2)		5.3, 3.1	

[a] Integration of all peaks gives expected integration. [b] δ-pyH and δ-CH_3 for complexes **1** or **2** and **3**, respectively. Integration values for δ-CH_3 are not reported due to the proximity of solvent peaks.

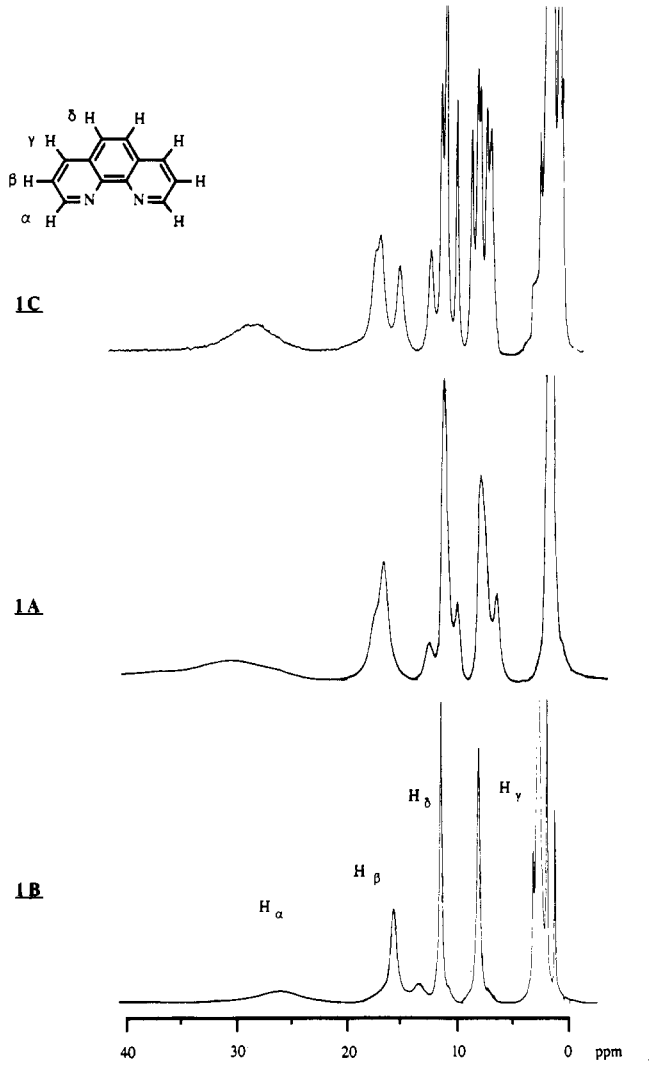

Figure 2. ^{1}H NMR spectra of $Fe_2O(Phen)_4Cl_2(ClO_4)_2$ (**1C**), $Fe_2O(Phen)_4(H_2O)_2(ClO_4)_4$ (**1A**) and $Fe_2O(Phen)_4(OAc)(ClO_4)_3$ (**1B**) in CD_3CN.

single peak. This was true also for the eight β, γ, or δ protons. In contrast, the protons were more differentiated in complex **1C**, while an intermediate differentiation was observed in complexes **1A** (or **1D**, data not shown). This might reflect different degrees of X ligand labilities, when complexes are dissolved in acetonitrile. When X is inert, exchange reactions with the solvent are very slow. This is the case when X = Cl. Thus, the solid-state structure remains in solution, and as shown from the three-dimensional structure of complex **1C**, the phenanthrolines remain magnetically nonequivalent, one trans and one cis to the oxo bridge. When X is labile, the exchange process is rapid and results in a high pseudosymmetry of the ^{1}H NMR spectrum, with all phenanthrolines becoming equivalent. This is the case when X = CH_3CO_2. At lower temperatures, the coalescence ceased to exist and the phenanthroline proton resonances became significantly more complex. The methyl protons of the acetate ligand were shifted to 10 ppm, indicating a monodentate coordination to iron (data not shown). Different species, with a nonbridging monodentate or a bridging bidentate acetate, might exist in rapid equilibrium with a shift to the latter at higher temperatures. This is the first direct observation of a labile acetate in μ-oxo diferric complexes. Recently a binuclear oxo-bridged Ru complex has been shown to undergo a rapid nonbridging monodentate–bidentate equilibrium of acetate ligands.[25] From our data, labilities of X ligands can be rated: CH_3CO_2 > H_2O > CF_3CO_2 > Cl. Accordingly, complex **1B** could be transformed into complex **1A**, during reaction with 5 equiv of water, and complex **1A** to **1B** during reaction with acetate, as proved by ^{1}H NMR spectroscopy. On the contrary, complex **1C** was unaffected by the presence of large excesses of water or acetate (data not shown).

UV–Visible Spectroscopy Studies. Electronic spectra were also sensitive to changes at the Fe–X coordination. Absorption spectra of complexes **1A-D** displayed bands that have been previously observed and characterized in spectra of (μ-oxo)diferric complexes (Figure 3).[1d] Data are collected in Table II. The UV region contained two strong transitions (ϵ > 9 mM^{-1} cm^{-1}) assigned to allowed oxo-to-iron charge transfers. These bands blue-shifted as the electron acceptor capacity of the X ligand increased. Only complexes **1A** and **1B** exhibited defined features in the 400–500-nm region, as previously observed for complex **4**. Finally, a broad and weak band (ϵ > 0.2 mM^{-1} cm^{-1}) was observed in the low-energy visible region. It has been previously assigned to a forbidden oxo-to-iron charge transfer and suggested to be correlated to the Fe–O–Fe angle.[26] This is also shown here with complexes **1C** and **1A** with Fe–O–Fe angles of 161 and 155°, respectively, and absorptions at 580 and 602 nm. Complex **1B** absorbs at 640 nm, a value which indicates a much lower Fe–O–Fe angle value. This supports the hypothesis of the acetate bridging as a bidentate ligand between the two iron atoms. The

(25) Ochi, T.; Sasaki, Y.; Yamaguchi, T.; Ito, T. *Chem. Lett.* **1991**, 2019.
(26) Norman, R. E.; Holtz, R. C.; Ménage, S.; O'Connor, C. J.; Zhang, J. H.; Que, L., Jr. *Inorg. Chem.* **1990**, *29*, 4629.

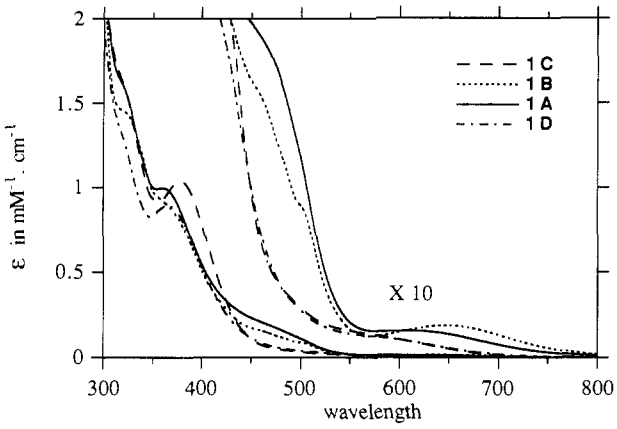

Figure 3. Electronic spectra of complexes **1A-D** in CH_3CN.

Fe–O–Fe angle value for previously reported (μ-oxo)(μ-carboxylato)diiron complexes is around 130°. We observed similar effects of the X ligands on the electronic absorption properties of complexes **2** and **3** (Table II).

Resonance Raman Studies. All complexes exhibited a strongly enhanced Fe–O–Fe symmetric stretching vibration in their resonance Raman solution spectra upon excitation into the oxo-to-iron charge transfer band (Table II). Under the present recording conditions, the asymmetric stretching mode was too weak to be detected. For complexes **A**, **C**, and **D**, the vibrational frequency was found at around 380 cm^{-1}, while it was found at 480 cm^{-1} for complexes **B**. The first value has been previously shown to be characteristic of monobridged diferric complexes while the second one is characteristic of dibridged complexes.[27] This strongly confirms the bridging binding mode of acetate in complexes **B**. Moreover, from the high frequency value it is possible to get an approximative Fe–O–Fe angle value of 135° for complex **1B**, according to previously reported correlations between the Fe–O–Fe stretching vibrational frequency and the Fe–O–Fe angle.[28,29] It should be noted that, in the case of complexes **3A** and **3D**, a Fermi resonance doublet, probably arising from the overlap of the symmetric Fe–O–Fe vibrational frequency with a combination band at the same frequency, was observed.[29]

Magnetic Studies. Variable-temperature magnetic susceptibility measurements were made on **1C** and **2B**. The fits of the data to the model of an isolated Heisenberg dimer of $S = {}^5/_2$ ions with the hamiltonian $\mathcal{H} = -2JS_1 \cdot S_2$ afforded a spin coupling J value of -113.3 ± 0.5 cm^{-1} and -118.7 ± 0.5 cm^{-1} for **1C** and **2B** respectively with $g = 2.0$. These values reflect the ability of the oxo bridge to mediate the spin coupling even in the presence of an additional carboxylate bridge.

In conclusion, all spectroscopic data showed that these (μ-oxo)diferric complexes, containing bidentate nitrogen ligands, bind only one acetate as a bridging bidentate ligand but bind one trifluoroacetate on each iron as a monodentate ligand. This is consistent with the differences in electron donor capacities between the two carboxylates.

Crystallographic Characterization of Complex 3D. The structure of the cation of **3D** is shown in Figure 4. As expected from spectroscopic results, the two ferric iron atoms are bridged by a single oxo ligand. Each iron atom has a N_4O_2 donor set, in a distorted octahedron, with four nitrogen atoms from two methylated bipyridines and one extra oxygen atom from a monodentate trifluoroacetate anion. It is rather remarkable that the carbonyl oxygen atom of the carboxylate lies above the plane of the bipyridine, suggesting stabilizing dipole interactions between the oxygen lone pairs and the pyridine π ring.

This structure is very close to that of the cation of complexes **1C** or **1A**, previously described.[17,21] In particular, the two chelate rings cis to the oxo bridge are nearly parallel to each other, developing stabilizing π stacking interactions. The Fe–oxo (1.786(7)Å) and Fe–N bond lengths are similar to the ones in **1C** (Table IV).[21] As in **1C**, a longer Fe–N distance is found for the two nitrogen atoms trans to the oxo bridge, reflecting the trans effect. A slightly smaller effect is observed for the Fe–N bonds trans to the carboxylates. The Fe–O bond length (1.997(6)Å) is not unusual for an iron–carboxylate bond. The carbonyl oxygen is over 3.47 Å from Fe in agreement with the monodentate coordination mode. The Fe–O–Fe angle is 163.0(3)°, similar to the one in **1C** but larger than the one in **1A**. Electronic repulsions between the negatively charged terminal ligands might be responsible for the increase of the angle. On the other hand, the π stacking of the two cis bipyridine groups may explain the deviation of the Fe–O–Fe angle from 180°. This geometry leads to a distance between the two iron atoms of 3.535 Å.

Only a few examples of structurally characterized Fe(III) complexes with a monodentate carboxylate ligand are known.[30] The only other oxo-bridged binuclear complex containing a monodentate carboxylate is $Fe_2O(BiPhMe)_2(HCO_2)_4$. However, in that case the anti lone pair is used to form the Fe-O bond.[31]

Catalytic Activity of the $Fe_2OL_4X_n(ClO_4)_m$ Binuclear Complexes. The catalytic activity of complexes **1–3** was tested during the oxidation of cyclohexane by *tert*-butyl hydroperoxide (TBHP) in acetonitrile under anaerobic conditions over a 30-min period. Under our standard conditions (0.7 mM Fe complex, 0.77 M C_6H_{12}, 0.1 M TBHP), oxidation of cyclohexane yielded cyclohexanol (cyOH) and cyclohexanone (cyONE) in relative amounts (Table V). Also, small amounts of *tert*-butyl cyclohexyl peroxide were formed while no bicyclohexyl could be detected. As expected, TBHP was also found to decompose to O_2 gas, a reaction competing with the oxidation of cyclohexane. Both reactions were dependent on the presence of the iron complex. To avoid oxygen in the incubation mixture, solutions were thus continuously bubbled with argon during the reaction or maintained under reduced pressure (30–40 mmHg). Experiments were also carried out in aerated solutions. In no case were the yields of the oxidation products significantly affected, demonstrating that oxygen was not involved in the reaction. Accordingly, cyclohexyl hydroperoxide could not be detected during the reaction. This was also demonstrated during oxidation of adamantane which was carried out under reduced pressure (10 mmHg). Moreover, addition of 0.1 M *tert*-butyl cyclohexyl peroxide to the complete reaction mixture had no effect on the product yields. In the absence of cyclohexane the dialkyl peroxide was very stable and reacted with the iron complexes only very slowly to give cyclohexanone, as the only product. These experiments show that *tert*-butyl cyclohexyl peroxide was not the precursor or the alcohol and the ketone. It also shows that in this system, hydroperoxides but not dialkyl peroxides can be used as oxidants. Furthermore, we demonstrated that cyclohexanol was not the precursor of cyclohexanone, even though cyclohexanol can be oxidized to cyclohexanone. Actually, addition of cyclohexanol to the complete reaction mixture did not affect the yield of cyclohexanone resulting from cyclohexane oxidation.

Complexes **1–2A** and **1–2B** gave nearly identical primary kinetic isotope effects for the activation of cyclohexane using C_6H_{12} and C_6D_{12} as substrates. Values around 8.5 and between 3.0 and 4.8 were determined for the formation of cyclohexanone and cyclohexanol respectively. These high values are comparable to

(27) Sanders-Loehr, J.; Wheeler, W. D.; Shiemke, A. K.; Averill, B. A.; Loehr, T. M. *J. Am. Chem. Soc.* **1989**, *111*, 8084.
(28) Turowski, P. N.; Armstrong, W. H.; Roth, M. E.; Lippard, S. J. *J. Am. Chem. Soc.* **1990**, *112*, 681.
(29) This phenomenon is also present in complex **4**.
(30) Ménage, S.; Que, L., Jr. *Inorg. Chem.* **1990**, *29*, 4293 and references therein.
(31) Tolman, W. B.; Liu, S.; Bentsen, J. G.; Lippard, S. J. *Inorg. Chem.* **1991**, *113*, 152.

Table II. Electronic Spectroscopic Properties and Vibrational characteristics of $Fe_2O(L)_4(X)_n(ClO_4)_m$ Complexes

	λ_{max} (ϵ)[a]					Fe–O–Fe stretch[b] ν_s
			L = Phen			
1A	330 (sh)	360 (10.0; sh)	460 (2.1)		602 (0.16)	388
1B	320 (14.5)	360 (sh; 9.2)	460 (1.5)	510 (sh; 0.84)	645 (0.19)	477
1C	325 (sh)	378 (10.4)			550 (0.16)	376
1D	330 (sh)	365 (9.0)		500 (sh)	570 (0.13)	386
			L = 22′Bipy			
2A	330 (sh)	360 (10.7)		500 (sh)	610 (0.14)	391
2B	330 (sh)	360 (sh;8.1)	460 (1.0)	500 (0.75)	640 (0.17)	480
2C	330 (sh)	372 (9.2)		480 (sh)	580 (sh; 0.14)	
2D	330 (sh)	360 (7.8)			570 (0.16)	384
			L = 44′Me_2 22′Bipy			
3A	330 (sh; 13.5)	360 (9.5)		500 (sh; 0.5)	610 (0.13)	378–405
3B	335 (14.3)	365 (9.6)	460 (1.2)	500 (0.8)	635 (0.18)	470
3C	305 (sh)	360 (11.7)			560 (0.16)	
3D	330 (sh)	360 (1.1)			570 (0.15)	379–397

[a] λ_{max} in nm (ϵ in mM^{-1} cm^{-1}). [b] ν_s(Fe-O-Fe) in cm^{-1} from resonance Raman spectra recorded in acetonitrile.

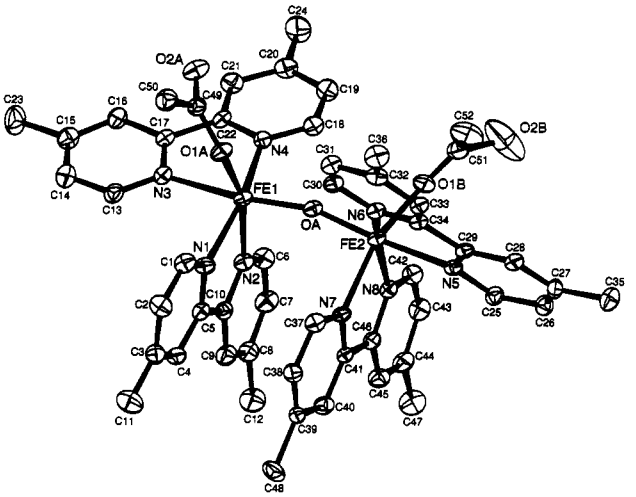

Figure 4. ORTEP representation of the structure of complex **3D** with 50% probability thermal ellipsoids. Hydrogen and fluorine atoms have been omitted for clarity.

Table III. Crystallographic Data for Complex **3D**

formula	$C_{56}H_{56}F_6Cl_2Fe_2N_8O_{15}$
fw	1377.3
temp, K	293
cryst syst	triclinic
space group	$P\bar{1}$
a, Å	14.690(2)
b, Å	15.583(2)
c, Å	16.260(2)
α, deg	74.05(1)
β, deg	66.59(1)
γ, deg	63.65(1)
V, Å^3	3038.5
Z	2
D(calc), g cm^{-3}	1.511
cryst dim, mm	0.2 × 0.2 × 0.2
radiation	Mo Kα (λ = 0.710 69 Å)
monochromator	graphite
μ, cm^{-1}	6.18
scan type	ω
2θ range, deg	1–50
h, k, l collcd	±17, ±18, +19
no. of reflns collcd	9970
no of indep refins used in refinement	7235
R[a]	0.083
R_w[a]	0.063

[a] $R = (\Sigma|(F_o - F_c)|)/(\Sigma F_o)$; $R_w = \langle(\Sigma w|F_o - F_c|^2)/(\Sigma w(F_o)^2)\}^{1/2}$.

those reported for iron porphyrin systems[32] and during methane oxidation by methane monooxygenase from *Methylococcus capsulatus*.[33]

Table IV. Selected Bond Lengths (Å) and Angles (deg) for **3D**[a]

	(a) Bond Lengths		
Fe1–OA	1.786(7)	Fe1–O1A	1.985(6)
Fe2–OA	1.789(7)	Fe2–O1B	1.995(6)
Fe1–N1	2.140(7)	Fe1–N2	2.165(8)
Fe1–N3	2.186(9)	Fe1–N4	2.108(6)
Fe2–N5	2.219(8)	Fe2–N6	2.122(7)
Fe2–N7	2.152(7)	Fe2–N8	2.145(8)
O1A–C49	1.262(13)	C49–O2A	1.221(10)
O1B–C51	1.230(9)	C51–O2B	1.260(12)
Fe···Fe	3.535(7)		
	(b) Bond Angles (deg)		
OA–Fe1–N1	100.1(0.4)	OA–Fe1–N2	94.7(0.4)
OA–Fe1–N3	168.9(0.2)	OA–Fe1–N4	94.0(0.4)
OA–Fe1–O1A	96.8(0.4)	N1–Fe1–N2	74.9(0.3)
N1–Fe1–N3	90.7(0.4)	N1–Fe1–N4	161.6(0.2)
N1–Fe1–O1A	88.5(0.3)	N2–Fe1–N3	85.6(0.4)
N2–Fe1–N4	92.4(0.3)	N2–Fe1–O1A	161.2(0.2)
N3–Fe1–N4	74.9(0.4)	N3–Fe1–O1A	85.9(0.4)
N4–Fe1–O1A	101.5(0.3)	Fe1–OA–Fe2	163.0(0.3)
OA–Fe2–N5	168.5(0.3)	OA–Fe2–N6	93.9(0.4)
OA–Fe2–N7	94.4(0.3)	OA–Fe2–N8	100.8(0.4)
OA–Fe2–O1B	96.3(0.3)	N5–Fe2–N6	74.6(0.4)
N5–Fe2–N7	86.9(0.4)	N5–Fe2–N8	90.5(0.4)
N5–Fe2–O1B	85.6(0.3)	N6–Fe2–N7	92.0(0.3)
N6–Fe2–N8	161.0(0.3)	N6–Fe2–O1B	102.1(0.3)
N7–Fe2–N8	75.0(0.3)	N7–Fe2–O1B	161.7(0.3)
N8–Fe2–O1B	88.3(0.3)	Fe2–N5–C25	126.0(0.4)
O1A–C49–O2A	129.3(1.0)	O1B–C51–O2B	128.2(0.9)

[a] Estimated standard deviations in the least significant digits are given in parentheses.

Reactions were inhibited by CCl_4 and dimethyl sulfide (Table V). CCl_4 (cyclohexane:CCl_4 = 1:1.3) gave approximately a 50% inhibition during oxidation of cyclohexane in the presence of complex **1A**, without any effect on the ketone:alcohol ratio. Formation of chlorocyclohexane demonstrated the intermediate formation of substrate radicals in this reaction.[34]

Dimethyl sulfide ($(CH_3)_2S$:cyclohexane = 1:7.6) was also a very good inhibitor of cyclohexane oxidation (Table V). However, while the production of CyOH and CyONE was greatly lowered (around 80% inhibition, again without effect on the alcohol:ketone

(32) (a) Lindsay Smith, J. R.; Sleath, P. R. *J. Chem. Soc., Perkin Trans. 2* **1983**, 621. (b) Groves, J. T.; Nemo, T. E.; Myers, R. S. *J. Am. Chem. Soc.* **1979**, *101*, 1032. (c) Nappa, M. J.; McKinney, R. J. *Inorg. Chem.* **1988**, *27*, 3740. (d) Battioni, P.; Renaud, J. P.; Bartoli, J. F.; Reina-Artiles, M.; Fort, M.; Mansuy, D. *J. Am. Chem. Soc.* **1988**, *110*, 8462. (e) De Prooter, B.; Ricci, M.; Meunier, B. *Tetrahedron Lett.* **1985**, 4459.

(33) Rataj, M. J.; Kauth, J. E.; Donnelly, M. I. *J. Biol. Chem.* **1991**, *266*, 18684.

(34) (a) Hill, C. L.; Schardt, B. C. *J. Am. Chem. Soc.* **1980**, *102*, 6374. (b) Groves, J. T.; Nemo, T. E. *J. Am. Chem. Soc.* **1983**, *105*, 6243.

Table V. Products Distribution in the Oxidation of Cyclohexane by TBHP Catalyzed by Complexes 1–3

catalyst	products[a] cyOH	cyONE	cyOOtBu	Me_2SO or cyCl[b]	% yield[c]
			L = Phen		
1A	17	19	7		44
1A(+CCl_4)	8	7		7	20
1A(+Me_2S)	2	3	6	15	18
1B	18	13	5		35
1C	1	1	1		<2
1D	1	1			<2
			L = 22'bipy		
2A	17	19	7		44
2B	18	15	6		38
2C	1	1			<2
2D	1	1	1		<2
			L = 44'$Me_2$22'bipy		
3A	16	19	8		44
3B	27	24	7		57
3C	1	1	1		<2
3D	7	5	3		15

[a] Moles of product per mole of catalyst after complete reaction. [b] cyCl = chlorocyclohexane. [c] Total yield based on oxidant (error value ±2%). The ketone yields are molar yields multiplied by 2 since 2 equiv of TBHP are required to make one equivalent of ketone.

Table VI. Product Distribution in the Oxidation of Hydrocarbons by TBHP, Catalyzed by Complexes **2A,B**

substrate	catalyst	products	% yield[a]	TN[b]
adamantane	**2A**	1-adamantanol		24
		2-adamantanol	24	3
		2-adamantanone		4
adamantane	**2B**	1-adamantanol		22
		2-adamantanol	22	3
		2-adamantanone		3
toluene	**2A**	benzaldehyde	10	6
		benzylalcohol		1
benzylalcohol	**2A**	benzaldehyde	70	100
trans-stilbene	**2A**	*trans*-stilbene oxide	19	8
		benzaldehyde		11

[a] The reaction is completed after 30 min for adamantane and 15 min for the other substrates; total yield based on oxidant. [b] TN = mole of product per mole of catalyst.

ratio), the yield of *tert*-butylcyclohexyl peroxide was not affected. During the reaction $(CH_3)_2S$ was oxidized into dimethyl sulfoxide.

Complexes **A** and **B** were also active during oxidation of adamantane, toluene, benzylic alcohol, and stilbene, as shown in Table VI. In the case of adamantane, the limiting reactant was the substrate because of its low solubility in acetonitrile. The presence of *tert*-butyladamantanyl peroxides was not searched for but would account for the missing material since the mass balance was around 70%.

The new oxidizing system described in this paper displays the following general features. (i) With the observed high rates of reaction and good yields of oxidation products, it is the most efficient oxidizing system, using TBHP as the oxidant and a non-heme iron complex as the catalyst, described so far. (ii) The ketone:alcohol ratio is close to 1. A similar ratio has been obtained during oxidations catalyzed by $Fe(TPA)Cl_3$, a mononuclear iron complex.[35] With other systems, both higher (Gif system)[36] and smaller (monooxygenases such as cytochrome P450 or methane monooxygenase, iron porphyrin-based systems)[37] ratios were obtained. (iii) The C3/C2 ratio, determined during adamantane oxidation, was around 10. Smaller (Gif system or methane monooxygenase)[38] and higher (iron porphyrin systems)[39] values

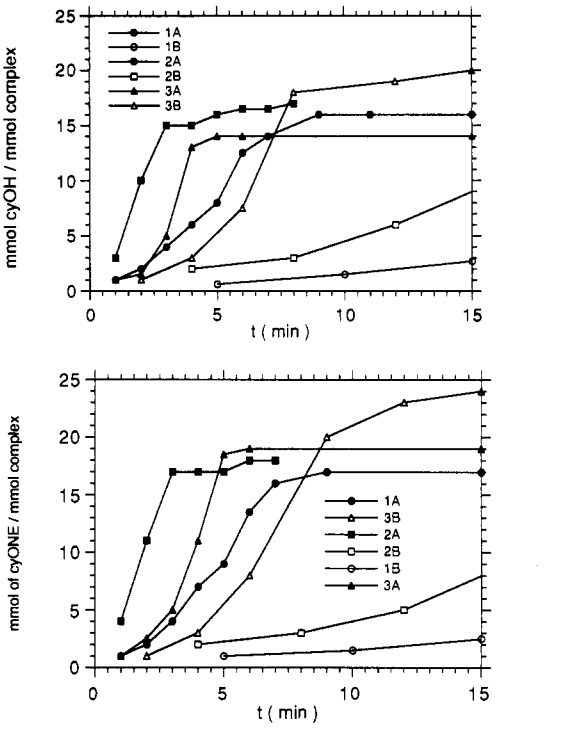

Figure 5. Cyclohexanone and cyclohexanol yields as a function of time in the oxidation of cyclohexane by TBHP in the presence of complexes **1A,B, 2A,B, 3A,B.**

were also reported. (iv) No aromatic hydroxylation could be observed during oxidation of toluene or benzene. All of these observations strongly suggest that hydroxyl radicals are not involved in the reaction.

Catalyst Structure/Reactivity Correlations. Table V shows that complexes **C** and **D**, carrying Cl or CF_3CO_2 as X ligands, were, in general, very poor catalysts, whatever the ligand L was. $FeCl_3$ was completely inactive while $Fe(ClO_4)_3$ allowed a slow but significant oxidation of cyclohexane by TBHP. The most active catalysts were complexes **A** and **B**, with X = H_2O or CH_3CO_2, with yields reaching approximately 50%, based on the consumed oxidant, the limiting reactant under the standard conditions. Complex **3B** gave a 57% yield.

In order to differentiate complexes **1A,B**, **2A,B**, and **3A,B** in greater detail we studied the time dependence of the reaction (Figure 5). At any time of the reaction CyONE and CyOH were formed in approximately equal amounts. The cyclohexanol did not precede cyclohexanone confirms that the latter was not derived from the former. The reaction stopped when TBHP was almost completely consumed, as checked by GC. The initial reaction rate appeared to be very sensitive to the nature of both L and X ligands. Figure 5 shows that complexes **A**, with X = H_2O, were more active than complexes **B**, with X = CH_3CO_2. The best catalyst was complex **2A**, with a high turnover number per minute (around 16 mmol of product per millimole of complex and per minute), the reaction being completed after 3–5 min. The rate of the reaction then decreased with **3A > 1A > 3B > 2B > 1B**. With **1B** and **2B** the reaction was completed after only 2 hours. One should note that **3D ≫ 1D, 2D** (Table V). The higher activity of complexes **3** might be explained by the stronger basicity of the methyl-substituted bipyridine ligand.

It is tempting to correlate the observed relative catalytic activities of the binuclear iron complexes to the previously

(35) Leising, R. A.; Norman, R. E.; Que, L., Jr. *Inorg. Chem.* **1990**, *29*, 2555.
(36) Barton, D. H. R.; Doller, D. *Acc. Chem. Res.* **1992**, *25*, 504.
(37) Mansuy, D.; Bartoli, J. F.; Chottard, J.-C.; Lange, M. *Angew. Chem., Int. Ed. Engl.* **1980**, *19*, 909.
(38) Gif system: Barton, D. H. R.; Csuhai, E.; Doller, D., Ozbalik, N.; Balavoine, G. *Proc. Natl. Acad. Sci. U.S.A.* **1990**, *87*, 3401. MMO: Green, J.; Dalton, H. *J. Biol. Chem.* **1989**, *264*, 17698.
(39) See for example: (a) Groves, J. T.; Nemo, T. E.; Myers, R. S. *J. Am. Chem. Soc.* **1979**, *101*, 1032. (b) Barton, D. H. R.; Gastiger, M. J.; Motherwell, W. B. *J. Chem. Soc., Chem. Commun.* **1983**, 731.

discussed relative labilities and exchangeabilities of the X ligand (vide supra). Thus active complexes were those containing accessible coordination sites (X = H_2O or CH_3CO_2, and X = CF_3CO_2 to a lesser extent, but not X = Cl). Such sites probably allow the iron ions to interact with and to activate the hydroperoxide. As a more general conclusion, dynamic chemical models of methane monooxygenase iron site should not contain an Fe–Cl bond as the only "free" coordination site. This bond is too strong to allow exchange with solvent and reactants. This is not the only parameter to consider. As shown below, differences were also observed in terms of the stability of the catalysts and might modulate the relative catalytic activities of the various complexes. For example, complexes **B** were in general found to be more fragile than complexes **A**. This might partly explain their lower activity.

Complexes **A** and **B** decomposed slowly in solution. The principal degradation complex during this reaction was found to be the mononuclear ferrous $[FeL_3]^{2+}$ complex. This was demonstrated by the appearance of the characteristic intense absorption bands at around 500 nm in the visible spectrum of the reaction mixture[40] and by the characteristic proton resonances in the diamagnetic region of the ^1H NMR spectrum. Addition of TBHP and substrate greatly accelerated the decomposition only in the case of complexes **1B** and **2B**. After 2 h of reaction, 30% of complex **1B** but only 8% of complex **1A** were transformed into the corresponding ferrous complex.

The formation of the ferrous complex, which was found to be inactive for catalysis, thus explains the slow inactivation of the catalysts. In one experiment, cyclohexane was allowed to react with TBHP in the presence of **1A** under standard conditions. At the end of the reaction the same amount of TBHP was added to the reaction mixture. Between 80% and 90% of the expected yield was then obtained during the second run. A third and fourth run gave 70% and 62% of the expected yield, respectively. At the end of the reaction, the other part of the iron was recovered as a binuclear iron species, retaining the Fe–O–Fe motif. This was shown by the absence of characteristic signals of mononuclear iron in the low-temperature EPR spectrum of the reaction mixture and by the characteristic resonances of the L ligand in the ^1H NMR spectrum. However, the shape and the position of the L protons signals were slightly modified, indicating a modification of the Fe–X coordination. It is possible that during the reaction X has been replaced by another ligand (solvent, oxidation products).

(40) Lever, A. B. P. In *Inorganic Electronic spectroscopy*, 2nd ed.; Elsevier: New York, 1984.

Conclusion

This work represents the first attempt to correlate the structure of non-heme binuclear iron complexes, as models of methane monooxygenase, and their catalytic activity during activation of C–H bonds by hydroperoxides. We have shown that this activity can be finely tuned by small modifications at the iron environment. An absolute requirement is the presence of an exchangeable coordination site which allows the oxidant to bind to the metal center. We found that a bidentate bridging acetate may also provide such a site. With some of our complexes, high turnover numbers and good yields were obtained, with only a limited and slow inactivation of the catalyst. This supports the present biomimetic strategy, based on binuclear rather than mononuclear complexes, used to design new oxidizing systems. Moreover, preliminary mechanistic studies suggest that alkyl radicals are intermediates during the oxidation of alkanes. OH• radicals and molecular oxygen do not appear to be involved in the reaction, suggesting that substrate-derived hydroperoxides are not reaction intermediates.[41,42] This greatly contrasts with the oxidations of alkanes by hydrogen peroxide catalyzed by binuclear iron complexes reported recently.[11] In that case, the reaction is better described as a metal-catalyzed autooxidation. On the other hand, the active species in the reaction reported here (high-valent iron–oxo or TBHP-derived oxy radicals)[43] cannot be identified yet. We are currently trying to improve the activity and stability of the catalysts and to understand the mechanism of the reaction in greater detail.

Acknowledgment. We thank Dr. J. Bonvoisin for performing the magnetic susceptibility experiments.

Supplementary Material Available: Tables of positional parameters (Table S2), anisotropic thermal parameters (Table S3), bond lengths and bond angles (Table S5, and Table S4, respectively) (14 pages). Ordering information is given on any masthead page.

(41) Barton, D. H. R.; Béviere, S. D.; Chavasiri, W.; Doller, D.; Bin Hu. *Tetrahedron Lett.* **1992**, *38*, 5473.
(42) Barton, D. H. R.; Béviere, S. D.; Chavasiri, W.; Csuhai, E.; Doller, D.; Liu, W.-G. *J. Am. Chem. Soc.* **1992**, *114*, 2147.
(43) Mansuy, D.; Battioni, P. In *Activation and Functionalization of Alkanes*; Hill, C. G., Ed.; Wiley-Interscience Publishers: New York, 1989; p 195.